APL MATERIALS **5**, 126106 (2017)

Depth distribution of secondary phases in kesterite Cu_2ZnSnS_4 by angle-resolved X-ray absorption spectroscopy

J. Just,[1,2] D. Lützenkirchen-Hecht,[2] O. Müller,[3] R. Frahm,[2] and T. Unold[1]

[1]*Department Structure and Dynamics of Energy Materials, Helmholtz-Zentrum Berlin für Materialien und Energie GmbH, Hahn-Meitner-Platz 1, 14109 Berlin, Germany*

[2]*Fakultät 4–Physik, Bergische Universität Wuppertal, Gaussstrasse 20, 42109 Wuppertal, Germany*

[3]*Stanford Synchrotron Radiation Lightsource (SSRL), SLAC National Accelerator Laboratory, Stanford University, Menlo Park, California 94025, USA*

(Received 15 August 2017; accepted 26 October 2017; published online 12 December 2017)

The depth distribution of secondary phases in the solar cell absorber material Cu_2ZnSnS_4 (CZTS) is quantitatively investigated using X-ray Absorption Near Edge Structure (XANES) analysis at the K-edge of sulfur at varying incidence angles. Varying information depths from several nanometers up to the full thickness is achieved. A quantitative profile of the phase distribution is obtained by a self-consistent fit of a multilayer model to the XANES spectra for different angles. Single step co-evaporated CZTS thin-films are found to exhibit zinc and copper sulfide secondary phases preferentially at the front or back interfaces of the film. © *2017 Author(s). All article content, except where otherwise noted, is licensed under a Creative Commons Attribution (CC BY) license (http://creativecommons.org/licenses/by/4.0/).*
https://doi.org/10.1063/1.5000306

Multinary chalcogenide materials such as Cu_2ZnSnS_4 (CZTS) exhibit widely tunable optical and electronic properties and have thus a great potential for a large variety of optoelectronic applications.[1,2] Due to its p-type semiconducting nature with an optical bandgap of 1.5 eV, CZTS has been increasingly promoted as an earth abundant absorber material for photovoltaics.[3–5]

However, due to the large number of constituent elements and thus the possibility for the formation of multiple phases, a quantitative knowledge about the formation of secondary phases is crucial for further developments.[6] Different techniques have so far been applied to identify secondary phases in CZTS such as X-ray diffraction (XRD),[7–10] Raman spectroscopy,[9,11–14] solid-state Nuclear Magnetic Resonance (NMR),[15] and X-ray absorption near edge spectroscopy (XANES).[16–19] While it has been found in numerous studies that the electronic properties of CZTS-based solar-cell devices correlate with the integral sample composition,[2,20–23] we have demonstrated recently that excess in zinc or copper will unavoidably lead to the segregation of the corresponding secondary phase, that is, zinc sulfide and copper sulfide.[17]

Secondary phases can have a significant influence on the electrical performance of the solar-cell device, depending on the spatial location of these segregations in the absorber layer. It is therefore of importance to investigate the depth distribution of secondary phases. Recent attempts using X-ray photoelectron spectroscopy have shown significant differences in surface composition with respect to the bulk composition of the material, which may be attributed to secondary phases.[24,25] Raman scattering and energy dispersive X-ray spectroscopy have been used to investigate the element and phase composition on the surface or interfaces of thin-films.[26,27] Further, Raman spectroscopy in conjunction with ion sputtering was used to investigate secondary phases depth.[14] While the above mentioned methods are useful to identify secondary phases in CZTS they however lack a quantitative measure.

As recently demonstrated, XANES at the K-edge of sulfur can be used to quantify the integral amount of secondary phases in CZTS with an accuracy of 3%.[16,17] Using X-ray fluorescence detection instead of transmission mode measurements as well as small incidence angles, the sensitivity of

 © Author(s) 2017

XANES to the detection of secondary phases can be further improved. Herein, we report a method based on X-ray absorption spectroscopy measured at different angles of the incident beam in conjunction with a multilayer based absorption model to quantitatively determine the depth distribution of secondary phases in CZTS thin-films.

The investigated CZTS thin-films are prepared by physical vapor deposition in a single-stage co-evaporation process of copper, zinc sulfide, tin, and sulfur at a nominal substrate temperature of 550 °C.[28] Molybdenum coated soda-lime glass is used as substrate. A thin-film copper sulfide reference film is deposited analogously and is scratched off to produce a powder reference sample for transmission measurements of the X-ray absorption fine structure. Stoichiometric powder reference samples of Cu_2ZnSnS_4 and ZnS were prepared by mechanical milling starting from the corresponding binary sulfides CuS, ZnS, and SnS followed by annealing steps in sealed evacuated silica tubes as well as H_2S-atmosphere at maximum temperatures of 800 °C and 500 °C. For details refer to Ritscher *et al.*[18] Because of their exact stoichiometric composition and high-temperature equilibration, the powder reference samples are assumed to consist of a single phase only.

The X-ray Absorption Near Edge Structure (XANES) of the powder reference samples at the K-edge of sulfur was measured at beamline A1 at the DORIS III synchrotron at HASYLAB[29] as well as at beamline KMC-1[30] at the BESSY synchrotron in transmission geometry as described elsewhere.[16] Thin-film samples were investigated by room-temperature in-vacuum XANES measurements by detection of the total fluorescence yield at beamline A1 at the DORIS synchrotron at HASYLAB, as further specified in the supplementary material.[29] A schematic of the sample environment and measurement geometry is shown in Fig. 1. The angle of the incident beam was varied between 0.4° and 90° while the position of the fluorescence detector was varied between 45° and 90°. For detection of the fluorescence intensity, a Passivated Implanted Planar Silicon (PIPS) detector was used. Due to the difficulty in sample preparation of powders for transmission measurements, possible thickness variations in the transmission sample may result in an amplitude reduction of the measured XANES oscillations. Therefore, the reference measurements of single phase powders are amplitude corrected by comparison with the thin-film reference samples which were measured in fluorescence geometry.

The absorption of the incident beam within the investigated sample as well as the self-absorption of the induced fluorescence radiation on its way to the detector leads to varying information depths

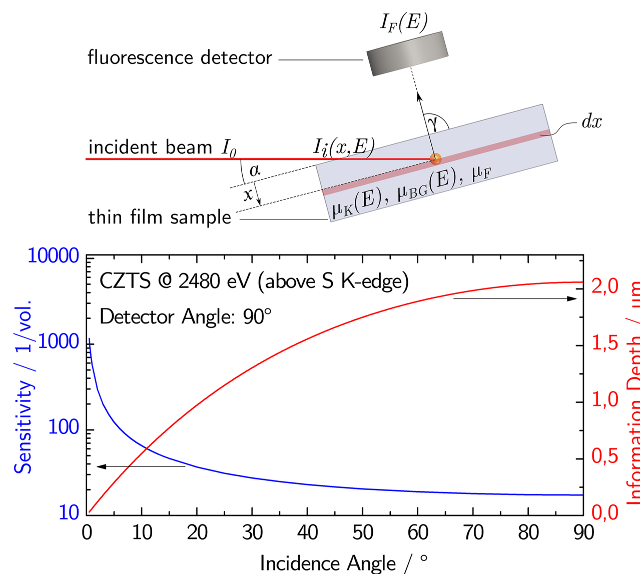

FIG. 1. Top: schematic of the geometry for the XAFS experiment with varying angles of the incident beam. Bottom: calculated information depth (right axis) of the K-edge XANES of sulfur in a CZTS sample for varying angles of the incident beam and a fixed detector angle of 90° to the surface. Additionally, the calculated sensitivity of this method to detect secondary phases in CZTS is shown (left axis), compare SEqs. (5) and (6) of the supplementary material.

depending on the measurement geometry. Due to the comparably high absorption of the incident beam as well as the fluorescence photons by the non-excited heavy cations, the information depth of the XANES can be varied from several nanometers of the surface to the entire thickness of the roughly 2 μm thick thin-films. The calculated information depth (90% of the fluorescence intensity of an infinitely thick sample) of a CZTS thin film for various angles of the incident beam based on tabulated X-ray absorption cross sections is shown in Fig. 1.[31] The sensitivity of this method to the detection of the secondary phases is based on the assumption that a deviation of 3% from the XANES spectrum of CZTS can be unambiguously identified as it was shown recently for transmission mode XANES measurements.[16] Therefore, the sensitivity of the measurement is maximized at the very surface for grazing incidence angles while it decreases significantly for buried phases, see Fig. 1. The value of the sensitivity gives the inverse of the fraction of a secondary phase which is needed within a 2 μm-thick sample in order to be detected within the information depth. If a secondary phase segregates at the surface, it can thus be detected at an incidence angle of 0.4° even if its total volume fraction is less than 0.07 vol. %, compare Fig. 1. Correspondingly, phase segregations extending to the centre of the bulk of a 2 µm thin-film sample can only be detected, if their amount exceeds 2.7% in volume. In order to reveal detailed information about phase segregations at the absorber back-contact interface, the measurements have been performed additionally on the same samples from the back side by detaching them from the molybdenum.

By a complete set of XANES measurements containing various angles of the incident and fluorescence beam the depth distribution of secondary phases can be reconstructed using a multilayer model. The absorption and emission model is constructed as follows: The intensity of the incidence beam penetrating into the sample can be described using Lambert-Beer's law with separated absorption coefficients for K-shell absorption μ_K(step-like) and continuous absorption μ_{BG} by the other shells of sulfur and the residual cations [SEq. (1), supplementary material]. The generated fluorescence radiation dF in an infinitesimally thick in-depth region dx is then proportional — with proportionality coefficient k — to the incident radiation that is absorbed by the K-shell of sulfur within this region [SEq. (2), supplementary material]. On its way to the detector the fluorescence radiation is attenuated with the absorption coefficient of the material at the energy of the fluorescence line μ_F. A detailed description of the derivation of the model can be found in the supplementary material. Such a combination of absorption, emission, and re-absorption of a thin-film of thickness d with the simplification of a point detector in the direction of the angle γ leads to the following description of the total measured fluorescence intensity $I_F(E)$ with an angle of the incident beam α:

$$I_F\,(d,E) = \int_0^d dF(x,E)\cdot e^{-\mu_F \frac{x}{\sin(\gamma)}},$$

with

$$dF\,(x,E) = k\cdot I_0\cdot \frac{\mu_K}{\sin(\alpha)} e^{-(\mu_{BG}+\mu_K)\frac{x}{\sin(\alpha)}}\,dx. \qquad (1)$$

The physical parameters on which the model is based [$\mu_K(E)$, $\mu_{BG}(E)$, and μ_F] are obtained from a combination of tabulated x-ray absorption cross sections[31] and measured reference spectra. While the continuous absorption coefficients $\mu_{BG}(E)$ and μ_F are directly taken from tabulated values, the step-like behavior of the tabulated $\mu_K(E)$ is superimposed by the measured XANES fine structure for every reference material, as illustrated in the supplementary material.

For a non-homogeneous material, i.e., a layer stack of different materials, the absorption coefficients μ_K, μ_{BG}, and μ_F are functions of the depth x. In the applied model, the integration over depth of a multilayer is performed numerically for 1000 steps in depth (dx).

Note that the measured spectra for different individual angles cannot simply be described as linear combinations of the reference spectra as the measured and edge-step normalized fluorescence intensity is not proportional to the linear absorption coefficient $\mu_K(E)$ which is measured in transmission mode. The measured spectra are significantly distorted from the reference spectra resulting in a reduced amplitude of the measured XANES oscillations compared to those of corresponding transmission spectra. Another distortion of the spectra results from the re-absorption of the generated fluorescence radiation on its way to the detector. Both effects are well described in the literature as self-absorption effects and can be corrected by several models.[32–35] These corrections do not have to be applied in this

work because all distortion effects are correctly described by the applied model. For geometric reasons as well as to achieve a high signal-to-noise ratio, the measurement was conducted by collecting the total fluorescence yield instead of the S-K_α fluorescence line only. Therefore, all calculations are performed assuming a second higher absorption coefficient for the outgoing low energy (L-line) fluorescence radiation additionally.

The described model considers absorption properties only and neglects surface and interface reflection which appears at very shallow angles of the incident beam. However, the reflectivity of a layer is strongly dependent on its roughness R_{RMS}, as shown in Fig. SI2 of the supplementary material. Simulations show that for an atomically flat surface of CZTS (R_{RMS} = 3 Å), the reflectivity is below 1% above incidence angles of 1.5° and can therefore be neglected for larger angles. For layers with a roughness above 20 nm RMS, which co-evaporated films typically exhibit, the reflectivity is below 1% for angles larger than 0.5° and can therefore be neglected for larger angles. Therefore, spectra measured below these angles are not included into the multi-layer fit. Further, the above described multi-layer model describes ideally flat surfaces and interfaces only. However, considering interface roughness as a pyramidal structure of material 1 with upward facing pyramids and material 2 with downward facing pyramids, it can be taken into account by introducing a linear gradient layer. This description is limited to a rough interface between *two* bulky materials. If the thickness of one layer is below the roughness of the surface or interface, the applied model reaches its limitations and results have to be interpreted carefully.

The edge-step normalized X-ray absorption spectra measured for an exemplary CZTS thin-film sample with elemental ratios Cu/Sn = 2.1 and Zn/Sn = 1.4 are shown in Fig. 2. It can clearly be seen that the phase distribution of the measured sample is far from being homogeneous and consists of at least three well distinguishable layers. The qualitative analysis already shows that the surface is dominated by copper sulfide, the bulk is dominated by CZTS, and ZnS segregates towards the back of the sample.

For a quantitative analysis, the whole dataset of a sample, containing all different measurement geometries, is fitted by using the above described multi-layer model. It is important to note that all modeling spectra are generated by one single multilayer model. In order to construct a feasible layer stack, an initial guess is made based on the qualitative evaluation of individual XANES spectra of different information depths. All individual layer thicknesses as well as mixture coefficients of phases are then simultaneously determined by least square fitting to the measured data set using the Levenberg-Marquardt algorithm, further details are given in the supplementary material.

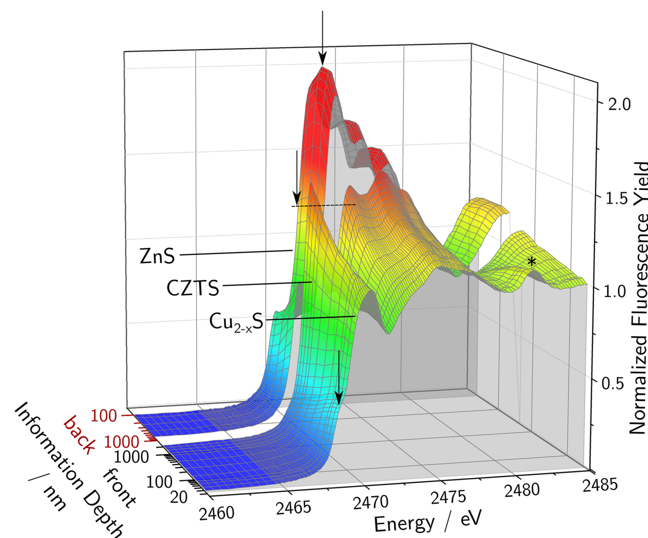

FIG. 2. Measured and edge step normalized fluorescence yield spectra of a typical co-evaporated CZTS sample for different incidence angles ranging from 0.5° (1.5°) to 90° (15°) from the front (back) surface. The arrows mark typical spectral features of the dominating phase. The peak (*) originates from S–O bonds due to surface oxidation.

The deduced multilayer model of one particular sample is shown in Fig. 3 together with measured spectra for different geometries and the self-consistent fits. For this particular sample, a three-layer model is able to describe the data measured for all different geometries nearly equally well. The electron microscope cross section image [Fig. 3(c)] was taken on a sample from the same deposition process. ZnS segregations appear white and are found at the bottom of the cross section, while small-sized copper sulfide precipitates are found at the surface, which is in good qualitative agreement with the deduced quantitative multi-layer model.

In order to check the consistency of the determined quantitative depth phase distribution model, the integrated phase composition is compared with the phase composition determined by linear combination analysis of the XANES measured in transmission geometry:[16] The specific sample shown in Fig. 3 consists of 1.8% copper sulfide, 11.3% zinc sulfide, and 86.9% CZTS according to the as determined multi-layer model. Linear combination analysis of the XANES measured in transmission geometry, which is also shown in Fig. 3, yields 2.1% copper sulfide and 10.5% ZnS, which is in excellent agreement taking the error of the measurement of about 3% by volume into account. The determined thickness of the copper sulfide segregation layer (55 nm) is far below the roughness of the surface, thus the applied simple multi-layer model can principally not accurately describe its absorption. However, the fit result gives a good estimate and is — within the errors of the measurement — consistent with both the integral transmission measurement and the qualitative microscope image.

All of the five investigated co-evaporated thin-film samples show significant segregations of secondary phases at the surface and the back of the absorber. For samples with an integral Cu/Sn ratio larger than one, copper sulfide was always found at the front surface, even if the Cu/(Zn + Sn)-ratio was below one. This is in agreement with previous quantitative observations of

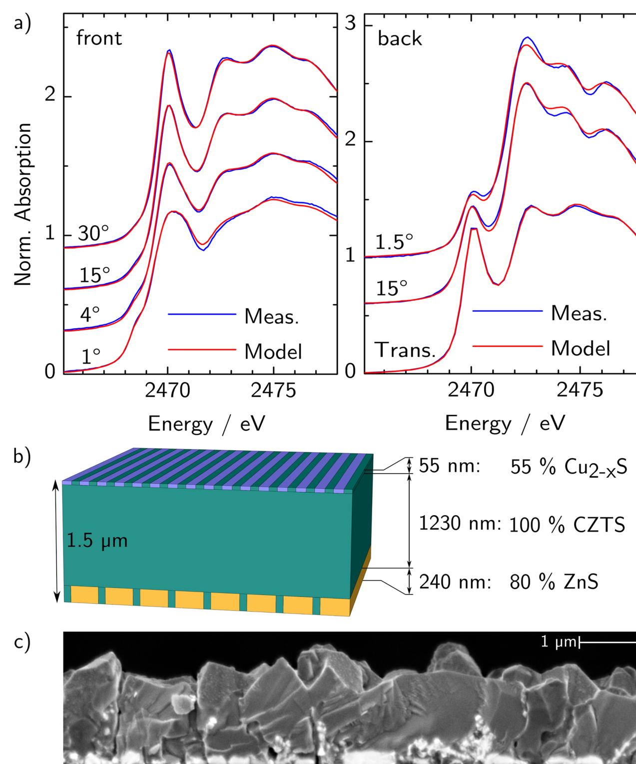

FIG. 3. (a) Measured and edge step normalized fluorescence yield spectra for several incidence angles from the front and the back of the sample in comparison with generated spectra by a multilayer model and pure phase reference spectra. For the integral phase composition, a transmission measurement of the same sample is shown additionally. (b) Scheme of the multi-layer model; quantitative measures are determined by least-square fitting to the whole set of measured spectra. (c) Electron microscope cross section image.

secondary phase segregations in CZTS which are shown elsewhere.[17] Segregations of the ZnS phase are also found to preferably appear at the front or the back surface for all investigated co-evaporated thin films: The concentration of ZnS in the surface near region by far exceeds the integrated concentration as measured by XANES in transmission mode. It therefore can be concluded — independent of the lower sensitivity of fluorescence detected X-ray absorption spectroscopy to bulk phases — that ZnS segregates preferably at the back and the front of single-stage co-evaporated CZTS films. For comparison, the phase composition was also measured for a CZTS sample produced by annealing in a high sulfur partial pressure atmosphere which was generously provided by the University of Uppsala.[36,37] The investigated sample was entirely Zn-rich (Zn/Sn = 1.18) and a total amount of 3.1% of ZnS by volume was detected by transmission XANES. In contrast to all co-evaporated samples, ZnS segregations are found to be homogeneously distributed over the entire depth of the thin film.

Considering solar cell devices, the impact of secondary phases on the electronic performance of the device can be much larger for phase segregations at the interfaces due to the formation of electronically unfavorable structures, i.e., a hole blocking layer of ZnS as it was directly observed recently by Wätjen *et al.*[38] A solar cell device was prepared from another co-evaporated sample from the same deposition process as the herein investigated one. It shows a poor power conversion efficiency of 2.2%, predominantly because of its low short circuit current density of 10.7 mA/cm^2, compared with a calculated current density of 33 mA/cm^2 which can be achieved with an AM 1.5 solar spectrum[41] and a bandgap of 1.5 eV. This reflects the current blocking behavior of the ZnS segregations which are found at the back contact. All investigated co-evaporated thin-film samples show segregations of copper sulfide and zinc sulfide preferably at the interfaces, thus the impact of such segregations is expected to be much higher than proportional to their volume fraction. The preferable segregation of copper sulfide on the front surface can be explained by its significantly different crystal structure compared to the kesterite structure and thus a minimization of the copper sulfide-kesterite interface area. Due to a nearly perfect lattice match between ZnS and CZTS, this argument does not hold for ZnS segregations. While the sample shown in Fig. 3 exhibits ZnS segregations only at the back, in other samples a small amount of ZnS was also found at the front. The preferable segregation of ZnS at the interfaces might be explained considering the known decomposition reactions of CZTS at elevated temperatures in vacuum (front) or in contact with molybdenum (back), where Cu_2ZnSnS_4 decomposes into elemental sulfur, tin monosulfide, zinc sulfide, and copper sulfide.[27,39,40] While the volatile products, sulfur and tin monosulfide, can re-evaporate from the surface and copper can diffuse into the Cu-poor bulk of the CZTS before it is saturated, ZnS will stay where it was released leading to the observed surface segregations. This interpretation is supported by the more homogeneous distribution of ZnS segregations in case of the high sulfur partial pressure treated CZTS sample which is not expected to show significant surface decomposition.

In summary, it was shown that quantitative depth information about the phase composition of CZTS thin-films can be revealed by angle-resolved measurements of the X-ray absorption near edge structure of the sulfur K-edge in conjunction with a fundamental absolute absorption model of a multi-layer structure. A whole dataset of spectra of a CZTS thin-film, measured for different geometries, can be accurately described by one single multi-layer model combining tabulated absolute absorption coefficients with measured X-ray absorption fine structures of single phase reference samples. It is furthermore shown that quantitative information about the depth distribution of secondary phases is obtained by self-consistent fitting of parameters of a multi-layer model to the complete dataset of spectra. As a consequence of different information depths for different measurement geometries, the applied method is much more sensitive to the detection of secondary phases at the surfaces of a sample than the recently demonstrated integrated detection by transmission measurements.[16] While an integral detection limit of 3 vol. % was claimed for transmission XANES, the detection limit for near-surface secondary phases using a grazing incidence geometry is anticipated to be as low as 0.09% by volume. In all investigated single step co-evaporated CZTS thin-films segregations of zinc sulfide and copper sulfide are found to be preferably at the front or back surface which might be explained by decomposition reactions at the CZTS-molybdenum or the CZTS-vacuum interface giving rise for the need of new process routines and back contact materials for CZTS solar cells.

See supplementary material for further details of the experimental setup, the applied multi-layer model, the fitting procedure, and simulations of the X-ray reflectivity.

The authors would like to gratefully acknowledge the provision of beamtime by HASYLAB and the Helmholtz-Zentrum Berlin (BESSY) as well as the support at the beamlines by Edmund Welter, Franz Schäfers, Mihaela Gorgoi, and Marcel Mertin. We gratefully acknowledge the provision of powder reference samples by Anna Ritscher of the Technische Universität Berlin. Furthermore, we would like to thank Tove Ericson and Jonathan Scragg from the University of Uppsala for the provision of a thin-film sample and inspiring discussions.

[1] T. Unold and H. W. Schock, Annu. Rev. Mater. Res. **41**, 297 (2011).
[2] K. Ito, *Copper Zinc Tin Sulfide-Based Thin Film Solar Cells* (John Wiley & Sons, 2015).
[3] K. Ito and T. Nakazawa, Jpn. J. Appl. Phys., Part 1 **27**, 2094 (1988).
[4] C. Persson, J. Appl. Phys. **107**, 053710 (2010).
[5] B. Shin, O. Gunawan, Y. Zhu, N. A. Bojarczuk, S. J. Chey, and S. Guha, Prog. Photovoltaics: Res. Appl. **21**, 72 (2013).
[6] A. Polizzotti, I. L. Repins, R. Noufi, S.-H. Wei, and D. B. Mitzi, Energy Environ. Sci. **6**, 3171 (2013).
[7] D. M. Berg, M. Arasimowicz, R. Djemour, L. Gütay, S. Siebentritt, S. Schorr, X. Fontané, V. Izquierdo-Roca, A. Pérez-Rodriguez, and P. J. Dale, Thin Solid Films **569**, 113 (2014).
[8] M. Ganchev, J. Iljina, L. Kaupmees, T. Raadik, O. Volobujeva, A. Mere, M. Altosaar, J. Raudoja, and E. Mellikov, Thin Solid Films **519**, 7394 (2011).
[9] A.-J. Cheng, M. Manno, A. Khare, C. Leighton, S. A. Campbell, and E. S. Aydil, J. Vac. Sci. Technol., A **29**, 51203 (2011).
[10] L. Choubrac, A. Lafond, C. Guillot-Deudon, Y. Moëlo, and S. Jobic, Inorg. Chem. **51**, 3346 (2012).
[11] P. A. Fernandes, P. M. P. Salomé, and A. F. da Cunha, Thin Solid Films **517**, 2519 (2009).
[12] A. Redinger, K. Hönes, X. Fontané, V. Izquierdo-Roca, E. Saucedo, N. Valle, A. Pérez-Rodríguez, and S. Siebentritt, Appl. Phys. Lett. **98**, 101907 (2011).
[13] E. A. Lund, H. Du, W. M. H. Oo, G. Teeter, and M. A. Scarpulla, J. Appl. Phys. **115**, 173503 (2014).
[14] X. Fontané, L. Calvo-Barrio, V. Izquierdo-Roca, E. Saucedo, A. Pérez-Rodriguez, J. R. Morante, D. M. Berg, P. J. Dale, and S. Siebentritt, Appl. Phys. Lett. **98**, 181905 (2011).
[15] M. Paris, L. Choubrac, A. Lafond, C. Guillot-Deudon, and S. Jobic, Inorg. Chem. **53**, 8646 (2014).
[16] J. Just, D. Lützenkirchen-Hecht, R. Frahm, S. Schorr, and T. Unold, Appl. Phys. Lett. **99**, 262105 (2011).
[17] J. Just, C. M. Sutter-Fella, D. Lützenkirchen-Hecht, R. Frahm, S. Schorr, and T. Unold, Phys. Chem. Chem. Phys. **18**, 15988 (2016).
[18] A. Ritscher, J. Just, O. Dolotko, S. Schorr, and M. Lerch, J. Alloys Compd. **670**, 289 (2016).
[19] Y. Cao, M. S. Denny, J. V. Caspar, W. E. Farneth, Q. Guo, A. S. Ionkin, L. K. Johnson, M. Lu, I. Malajovich, D. Radu, H. D. Rosenfeld, K. R. Choudhury, and W. Wu, J. Am. Chem. Soc. **134**, 15644 (2012).
[20] H. Katagiri, K. Jimbo, M. Tahara, H. Araki, and K. Oishi, MRS Proc. **1165**, M04 (2009).
[21] V. Kosyak, M. A. Karmarkar, and M. A. Scarpulla, Appl. Phys. Lett. **100**, 263903 (2012).
[22] S. Chen, A. Walsh, X.-G. Gong, and S.-H. Wei, Adv. Mater. **25**, 1522 (2013).
[23] J. Just, M. Nichterwitz, D. Lützenkirchen-Hecht, R. Frahm, and T. Unold, J. Appl. Phys. **120**, 225703 (2016).
[24] M. Bär, B.-A. Schubert, B. Marsen, S. Krause, S. Pookpanratana, T. Unold, L. Weinhardt, C. Heske, and H.-W. Schock, Appl. Phys. Lett. **99**, 152111 (2011).
[25] S. Harel, C. Guillot-Deudon, L. Choubrac, J. Hamon, and A. Lafond, Appl. Surf. Sci. **303**, 107 (2014).
[26] J. J. Scragg, T. Kubart, J. T. Wätjen, T. Ericson, M. K. Linnarsson, and C. Platzer-Björkman, Chem. Mater. **25**, 3162 (2013).
[27] J. J. Scragg, J. T. Wätjen, M. Edoff, T. Ericson, T. Kubart, and C. Platzer-Björkman, J. Am. Chem. Soc. **134**, 19330 (2012).
[28] B.-A. Schubert, B. Marsen, S. Cinque, T. Unold, R. Klenk, S. Schorr, and H.-W. Schock, Prog. Photovoltaics: Res. Appl. **19**, 93 (2011).
[29] E. Welter, AIP Conf. Proc. **1234**, 955 (2010).
[30] F. Schaefers, M. Mertin, and M. Gorgoi, Rev. Sci. Instrum. **78**, 123102 (2007).
[31] B. L. Henke, E. M. Gullikson, and J. C. Davis, At. Data Nucl. Data Tables **54**, 181 (1993).
[32] D. L. Brewe, D. M. Pease, and J. I. Budnick, Phys. Rev. B **50**, 9025 (1994).
[33] S. Eisebitt, T. Böske, J.-E. Rubensson, and W. Eberhardt, Phys. Rev. B **47**, 14103 (1993).
[34] C. H. Booth and F. Bridges, Phys. Scr. **2005**, 202.
[35] E. A. Stern and K. Kim, Phys. Rev. B **23**, 3781 (1981).
[36] T. Ericson, J. J. Scragg, T. Kubart, T. Törndahl, and C. Platzer-Björkman, Thin Solid Films **535**, 22 (2013).
[37] T. Ericson, T. Kubart, J. J. Scragg, and C. Platzer-Björkman, Thin Solid Films **520**, 7093 (2012).
[38] J. T. Wätjen, J. Engman, M. Edoff, and C. Platzer-Björkman, Appl. Phys. Lett. **100**, 173510 (2012).
[39] J. J. Scragg, T. Ericson, T. Kubart, M. Edoff, and C. Platzer-Björkman, Chem. Mater. **23**, 4625 (2011).
[40] A. Weber, R. Mainz, and H. W. Schock, J. Appl. Phys. **107**, 13516 (2010).
[41] ASTM G173-03(2012), Standard Tables for Reference Solar Spectral Irradiances: Direct Normal and Hemispherical on 37° Tilted Surface (ASTM International, West Conshohocken, PA, 2012).